COMMUNICATION

Check for updates

P3-type $K_{0.33}Co_{0.53}Mn_{0.47}O_2\cdot0.39H_2O$: a novel bifunctional electrode for Na-ion batteries†

Sai Wang,[ab] Tao Sun,[bc] Shuang Yuan,[b] Yun-hai Zhu,[ab] Xin-bo Zhang, [ID][b] Jun-min Yan [ID] *[a] and Qing Jiang [ID][a]

A novel electrode material, P3-type $K_{0.33}Co_{0.53}Mn_{0.47}O_2\cdot0.39H_2O$ (KCM), is synthesized through an easily-operated sol–gel method and it delivers considerable Na ion storage abilities when employed as both a cathode and an anode in NIBs. As a cathode, the compound displays remarkable average voltage potentials (over 3 V) and a high discharge capacity (114 mA h g^{-1} at 100 mA g^{-1}). As an anode, a safe and ideal average voltage potential (0.53 V), a high discharge capacity (174 mA h g^{-1}), and a long cycle life (950 cycles at 500 mA g^{-1}) are also delivered together. In addition, a KCM-based full cell is subsequently built and even without any optimization it can still exhibit a high energy density (91 W h kg^{-1}) accompanied by a long cycle performance (100 cycles at 100 mA g^{-1}).

Lithium-ion batteries (LIBs) are considered as promising renewable energy storage systems and have also become ubiquitous in our daily life as the power sources for portable electric devices, hybrid vehicles and electric vehicles.[1,2] However, the high price and the low availability of lithium sources might hinder the application of LIBs in the future. In this regard, the low cost and ubiquity of sodium sources make Na ion batteries (NIBs) an excellent alternative to LIBs, especially for large-scale applications.[3–5] Nevertheless, the larger radius and the heavier mass of Na ions make it hard to find suitable cathode/anode materials with satisfactory electrochemical performance for NIBs.[6–10] Furthermore, using the same process to produce the active material that could be employed both as cathode and anode materials would significantly decrease the manufacturing cost, but the development of such materials with superior Na ion storage ability is an enormous challenge and reports on such bifunctional electrode materials are still rarely seen.[11,12]

Conceptual insights

As a proof-of-concept experiment, this work firstly investigated the potential for electrochemical sodium storage of P3-type K_xMeO_2 (Me = transition metal), a rather unexplored family of electrode materials. In particular, exploring the electrochemical performances of $K_{0.33}Co_{0.53}Mn_{0.47}O_2\cdot0.39H_2O$ (KCM) as both a cathode and anode material provides a conceptual advance in the field of sodium-ion batteries (NIBs), where so far one material can only be employed as one kind of electrode (anode or cathode). Furthermore, in theory, P3-type K_xMeO_2 with a relatively low K content ($x \leq 0.5$) overcomes the space limitation for sodium accommodation/diffusion in MeO_6 sheets in the crystal structure of conventional high alkali content P2/O3-type Na_xMeO_2 electrode materials. Finally, since KCM belongs to a big family of P3-type A_xMeO_2 materials, this first example of the successful facile and scalable sol–gel synthesis and application of KCM in full-cell NIBs as well as the obtained promising electrochemical results and scientific understanding would provide a design principle and encourage more research on other high-performance and low cost bifunctional electrodes for next-generation high energy density NIBs.

The layered sodium transition metal oxides (Na_xMeO_2, Me = transition metal) with P2 ($x = 0.6$–0.7) and O3 ($x = 1$) structures have attracted extensive research interest as potential cathode materials for NIBs due to the easy preparation methods and high electrochemical performances.[13,14] However, in theory when the P2/O3-type Na_xMeO_2 materials are employed as anodes for NIBs, there would not be enough room to accommodate the inserted ions for further reduction reactions, thus resulting in limited capacities. In contrast, P3-type Na_xMeO_2 or K_xMeO_2 ($x \leq 0.5$) could both deliver and accommodate ions and thus should be a potential candidate for bifunctional electrode (cathode/anode) materials of NIBs. To our knowledge, there is no report on the precise synthesis, structural analysis and Na ion storage ability (either as a cathode or an anode) of P3-type K_xMeO_2, let alone on the bifunctional electrode performance for NIBs. Hence, developing a convenient and facile method to synthesize pure-phase K_xMeO_2 with P3 structure and then explore its comprehensive electrochemical performance in a broad voltage range for both cathodes and anodes is of great significance.

[a] Key Laboratory of Automobile Materials, Ministry of Education and Department of Materials Science and Engineering, Jilin University, Changchun 130012, P. R. China. E-mail: junminyan@jlu.edu.cn
[b] State Key Laboratory of Rare Earth Resource Utilization, Changchun Institute of Applied Chemistry, Chinese Academy of Sciences, Changchun, 130022, P. R. China
[c] University of Chinese Academy of Sciences, Beijing 100049, P. R. China
† Electronic supplementary information (ESI) available. See DOI: 10.1039/c7mh00512a

Herein, as a proof-of-concept experiment, a novel electrode material, $K_{0.33}Co_{0.53}Mn_{0.47}O_2 \cdot 0.39H_2O$ (KCM) with P3-type structure, is prepared through a convenient and mild sol–gel method, and is further tested in two different voltage ranges for exploring its overall Na ion storage ability as both a cathode and an anode. As was expected, in the voltage range of 1.6 and 4.6 V, an average voltage potential over 3 V together with a high discharge capacity of 114 mA h g^{-1} at 100 mA g^{-1} is delivered. Between 0 and 2 V, in addition to an ideal average voltage potential of 0.53 V and a considerable discharge capacity of 174 mA h g^{-1} (compared with other bifunctional electrodes), a long life cycle performance over 950 cycles with a reversible capacity of 73 mA h g^{-1} at 500 mA g^{-1} is also achieved. Furthermore, an innovative KCM-based Na ion full battery is later successfully assembled, which delivers a high energy density of 91 W h kg^{-1} and a remarkable cycle performance over 100 cycles.

A simple sol–gel method with CH_3COOK, $Co(CH_3COO)_2 \cdot 4H_2O$, $Mn(CH_3COO)_2 \cdot 4H_2O$ and citric acid as precursors was applied to synthesize the P3-type KCM. Previous reports have indicated that the potassium transition metal oxides are hygroscopic in the atmosphere and combine with water and form hydrated phases, thus exhibiting dehydration upon mild heating.[15,16] The total content of adsorbed water and structured water in the chemical formula is confirmed by the weight loss (6.4%) below 160 °C as revealed by thermogravimetric analysis (TGA) (Fig. S1, ESI†). Inductively coupled plasma-atomic emission spectroscopy (ICP-AES) was performed on the solution of the dissolved sample in the mixed solvent of concentrated sulfuric acid, hydrochloric acid and nitric acid (volume ratio 5:3:1), which indicates that the elemental stoichiometry of K, Co and Mn is 0.33:0.53:0.47. On the basis of the TGA and ICP-AES results and the general chemical formula (A_xMeO_2, A = alkali metal),[17] it is inferred that the chemical formula of the as-synthesized material is $K_{0.33}Co_{0.53}Mn_{0.47}O_2 \cdot 0.39H_2O$.

The crystalline phase structure of KCM was confirmed by X-ray diffraction (XRD) and the corresponding Rietveld refinement results are displayed in Fig. 1. The Bragg positions are strongly related to the cobalt oxyhydroxides prepared by Delmas's group,[18] and the result shows that the lattice parameters are $a = b = 2.8296$ Å, and $c = 20.3386$ Å ($R_{WP} = 2.65\%$, $R_p = 1.81\%$, $\chi^2 = 2.363$). The length of the c-axis lattice parameter is much larger than that of the P3-type Na_xMeO_2 materials which is more favorable for the easy insertion of Na ions. Tables S1 and S2 (ESI†) exhibit the calculated lattice reflections, inter-planar distances, peak intensities and atomic positions. Furthermore, from the inset of Fig. 1, it is observed that KCM belongs to the $R3M$ space group and crystallizes as P3-type with AABBCC oxygen packing. The oxygen atoms form octahedral positions and trigonal prismatic positions for transition metal ions and potassium ions, respectively. The trigonal prism shares one face with the adjacent octahedron and edges with the other three adjacent octahedrons in the next sheet.[17] The P3 type offers only one kind of intercalated site which is quite different from the P2 type structure which has two different prismatic positions. X-ray photoelectron spectroscopy (XPS) analysis was further performed to probe the valence states of KCM. Co $2p_{1/2}$
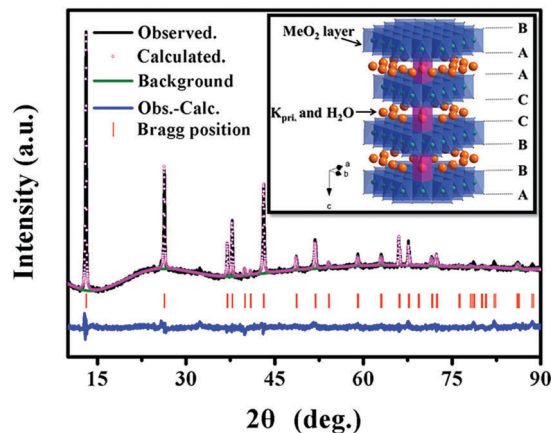

Fig. 1 Rietveld refinement patterns of X-ray diffraction data for KCM; the inset shows the refined crystal structure of KCM.

is fitted into peaks of 796.23 and 795.24 eV for Co^{2+} and Co^{3+}, respectively. Meanwhile the two fitted peaks located at binding energies of 780.82 and 780.01 eV are attributed to Co^{2+} $2p_{3/2}$ and Co^{3+} $2p_{3/2}$ (Fig. S2a, ESI†). The mole ratio of $Co^{2+}:Co^{3+}$ in KCM is about 1.05:1, indicating that the averaged valence state of cobalt is approximately +2.55. The XPS of the standard Co_3O_4 sample is also shown for comparison (Fig. S3a, ESI†).[19] Also, the two strong peaks of Mn 2p appearing at binding energies of 653.9 eV (Mn $2p_{1/2}$) and 642.3 eV (Mn $2p_{3/2}$) are close to those of the standard MnO_2 sample (653.7 and 641.9 eV) (Fig. S2b and S3b, ESI†), and this result indicates that the valence state of Mn is close to +4.[20] The broad O1s peak is fitted by four separate peaks at 532.15, 530.9, 529.7 and 529.05 eV that can be attributed to the existence of –OH, K–O, Co–O and Mn–O bonds, respectively[19,21,22] (Fig. S4a and b, ESI†).

The morphology and microstructure of the KCM particles were characterized by scanning electron microscopy (SEM) and high-resolution transmission electron microscopy (HRTEM). Fig. 2a presents the SEM image of KCM; it can be seen that KCM particles connect to one another and are in the size range of 50 to 500 nm. The HRTEM image (Fig. 2b) shows a set of parallel fringes with a spacing of 0.24 nm, corresponding to the
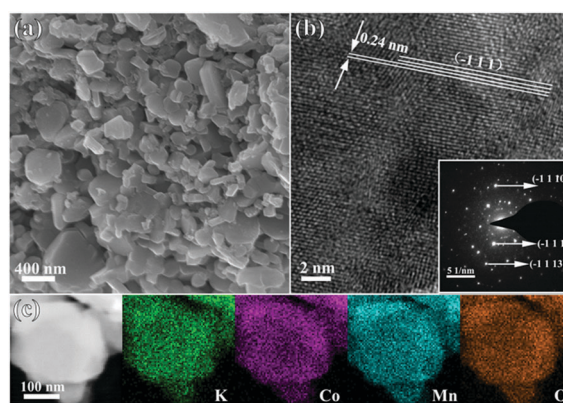

Fig. 2 (a) SEM image of KCM. (b) HRTEM image and SAED patterns (inset) of KCM. (c) Elemental mapping images of KCM.

(−1 1 1) plane of crystalline KCM according to the XRD analysis (Table S1, ESI†). The selected area electron diffraction (SAED) pattern also shows traces of various lattice planes of the KCM crystalline phase (Fig. 2b, inset). Elemental mapping images of the KCM particle (Fig. 2c) illustrate the homogeneous distribution of potassium, cobalt, manganese and oxygen.

The sodium storage abilities of KCM are evaluated by galvanostatic charge–discharge measurements with Na foils as the counter electrodes. KCM exhibits a charge capacity of 71 mA h g^{-1} in the first charge process, which indicates that approximately 0.27 ions per formula deviate from the trigonal prismatic positions according to Faraday's law. An activation process is obviously observed where the discharge capacity gradually increases from 92 to 114 mA g^{-1} (1st to 10th cycle) (Fig. 3a). This phenomenon could be explained by the gradual substitution of Na ions for K ions and is simultaneously related to the gradually decreasing charge-transfer resistance and increasing Na ion diffusion coefficient (Fig. S5 and Table S3, ESI†).[15] Therefore, both the residual K ions and the inserted ions are involved in the charge process from the 2nd cycle (95 mA g^{-1}) to the 10th cycle (123 mA g^{-1}). It needs to be emphasized that the average voltage potentials are all over 3 V. The *ex situ* XPS method was used to detect the chemical valence changes of the transition metal elements in the first charge process, and the detailed description is displayed in the ESI† (Fig. S6). The charge process is quite complicated and it is inferred that the oxidation of Co^{2+} to Co^{3+}, the activation of Mn^{4+} to Mn^{3+} and the cathode electrolyte interface (CEI) film forming process are involved. Activation processes are also observed at higher current densities of 200 and 500 mA g^{-1}, and maximum discharge capacities of 90 and 70 mA h g^{-1} are

delivered, respectively. After the activation process, KCM shows coulombic efficiencies of *ca.* 100% and reversible capacities (charge/discharge) of 80/79 mA h g^{-1} at 100 mA g^{-1}, 65/64 mA h g^{-1} at 200 mA g^{-1}, and 55/54 mA h g^{-1} at 500 mA g^{-1} are still delivered after 130 cycles (Fig. 3b). Moreover, KCM also exhibits an excellent rate performance, delivering discharge capacities of 110, 94, 73, 58, and 40 mA h g^{-1} at current densities of 100, 200, 500, 1000, and 2000 mA g^{-1}, respectively. Considerable discharge capacities above 95 mA h g^{-1} and stable cycles are obtained when the current density returns to 100 mA g^{-1} (Fig. 3c).

It is noticeable that the interplanar distance of 6.7795 Å is even larger than that of the typical carbon anodes for NIBs, and the non-stoichiometric chemical formula made it possible to accommodate more inserted ions and facilitate further conversion/deconversion reactions, so further testing in a lower voltage range (0–2 V) for the anodes of NIBs is performed. Fig. 3d shows the galvanostatic discharge/charge curves of KCM at 100 mA g^{-1}. As shown, it exhibits a discharge capacity of 479 mA h g^{-1} and a charge capacity of 173 mA h g^{-1} at the first cycle with ideal and safe average voltage potentials at approximately 0.53 V in the subsequent cycles. It is known from the initial high discharge capacity that the role of KCM as an anode is complex in that both insertion/desertion and conversion/deconversion mechanisms should be involved. The phenomenon that the capacity (1st discharge) deviates from the theoretical value should be most possibly caused by the formation of a solid electrolyte interface (SEI) film. At the same time, the conversion reaction from Co^{2+}/Co^{3+} to metal cobalt which is accompanied by the formation of Na_2O is proved to be achievable through *ex situ* XPS methods (Fig. S7, ESI†).[23] In the corresponding charge process, Mn^{2+} and Co are oxidized together with the decomposition of Na_2O. A number of K ions should also contribute to the specific charge capacity and form Na–K alloy on the counter electrode.[24–26] During the subsequent cycles, a maximum discharge capacity of 174 mA h g^{-1} is delivered (34 cycle) and a considerable cycle performance of 200 cycles with a retained capacity of 149 mA h g^{-1} is obtained. Further tests at higher current densities indicate that discharge capacities of 107 and 73 mA h g^{-1} are still exhibited even at 200 and 500 mA g^{-1} after 500 and 950 cycles, respectively (Fig. 3e). Fig. S8 (ESI†) shows the CV curves of the as-prepared KCM at a scan rate of 0.1 mV s^{-1} in the voltage range of 0–2 V, which correspond to discharge/charge curves with the same oxidation–reduction trends as the proofs. From the rate test result, it is known that the KCM electrode is able to deliver discharge capacities of 167, 134, 92, and 60 mA h g^{-1} at current densities of 100, 200, 500, and 1000 mA g^{-1}, respectively. When the current density is changed back to 100 mA g^{-1}, capacities above 165 mA h g^{-1} are still exhibited, demonstrating the superior rate ability of KCM (Fig. 3f). It is important to emphasize that except for the ideal average voltage potentials for both the cathode and anode, when compared with other published results on bifunctional electrodes, the cathode capacity presented here is close to the highest value and the anode capacity is more than double other published reports (Table S3, ESI†).
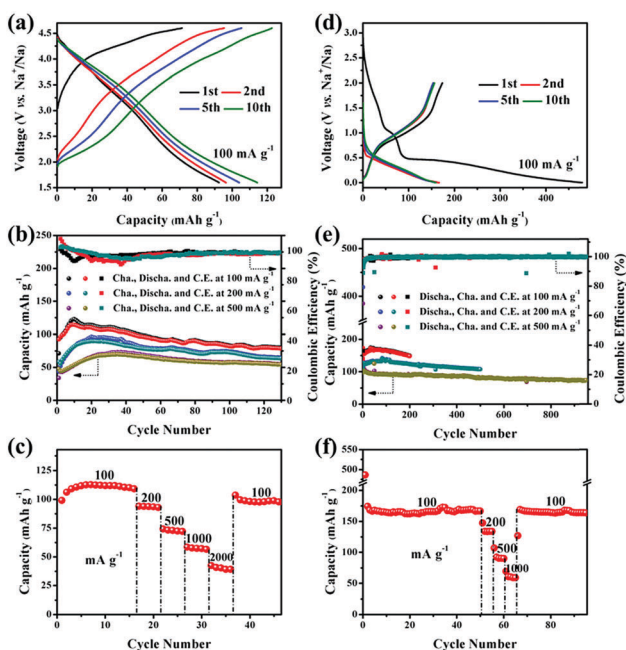

Fig. 3 (a and d) Typical charge–discharge/discharge–charge curves; (b and e) cycle performance; (c and f) rate capacity of KCM between 1.6 and 4.6 V (a–c) or 0 and 2 V (d–f).
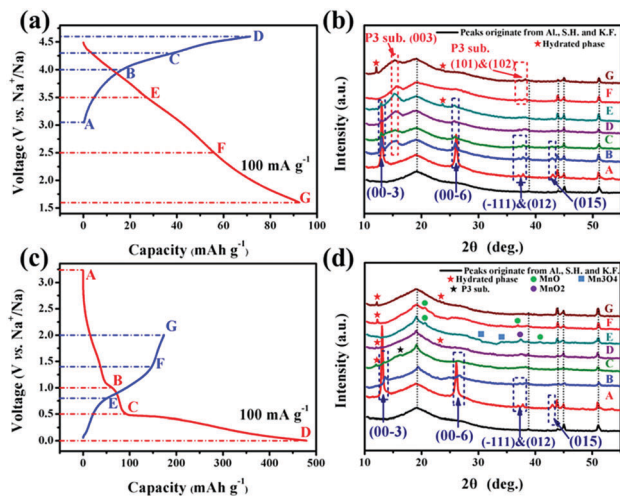
Fig. 4 (a and c) Initial charge–discharge/discharge–charge curves of KCM at 100 mA g^{-1} as the cathode/anode, electrodes with different charge/discharge depths are marked as A to G. (b and d) The corresponding XRD patterns of A to G states in (a) or (c).

The structure transformation mechanisms of KCM as a cathode and an anode for NIBs were further examined through *ex situ* XRD characterization of various charged and discharged electrodes at 100 mA g^{-1} with different voltage cutoffs (Fig. 4). A bare aluminum current collector sealed in a sample holder with a Kapton film window is first recorded as a reference and the patterns are marked as black lines in Fig. 4b and d. When the electrode is charged from open-circuit voltage (A point) to 4.0 V (B point), the peaks at 2θ degrees of 13° (0 0 −3) and 26° (0 0 −6) both decrease obviously and a peak at 15.6°, which corresponds to a 5.68 Å interplanar spacing, emerges (Fig. 4a and b). It is reported that the P2 and P3 type structures of Na$_x$MeO$_2$ show nearly the same highest interplanar spacing values that are all close to that of the newly-formed phase.[13,27] Nevertheless, the breaking of Me–O bonds cannot be realized without a high temperature environment, thus the phase transition from the P3 to P2-type phase is impossible.[28] Also, due to the fact that the insertion reaction of Na ions does not occur in the first charge process, it is deduced that the lattice of KCM contracts which leads to the formation of a new P3-type substitution. As the voltage reaches 4.3 V (C point), the peaks representing KCM get weaker and except for the P3-type substitution no more new phases are detected. At a charge cutoff of 4.6 V (D point), a weak signal at 13° that corresponds to the (0 0 −3) crystal plane is still detectable, and this phenomenon agrees well with the above-mentioned incomplete K ion desertion at the end of the first charge process. When the KCM electrode is first discharged to 3.5 V (E point), the formation of the peak at 23.7° could be explained based on the formation of some hydrated phases, and the water molecules originate from KCM. But at the same time the ion insertion reaction should also occur and is mainly contributed by Na ions. With continuous discharge to 2.5 V (F point), the KCM phase is almost undetectable. It is inferred that the ion-exchange of K ions with Na ions should be responsible for such an unusual

phenomenon. Further concentration polarization of Na ions between the two electrodes that arises from the deep discharge process is beneficial to the ion-exchange, and leads to lattice contraction resulting in the undistinguished XRD peaks of the pristine phase. At the end of the 1.6 V discharge (G point), besides the P3 substitution, another diffraction peak at 12.1°, which could be indexed to the insertion of water molecules, is also found. A common phenomenon for the 2nd and 20th cycles is observed that the hydrated phase vanishes as the voltage is recharged to 3 V and appears as the voltage is discharged to 1.6 V. In addition, based on the other *ex situ* XRD patterns of the 2nd cycle, it is summarized that the P3 substitution always exists and the vanished KCM no longer reappears (Fig. S9a and b, ESI†). Thus there are no drastic structure transformations that happen besides formation of some hydrated phases when KCM plays a role as a cathode of NIBs.

XRD patterns of the KCM electrodes recorded at different depths between 0 and 2 V are displayed in Fig. 4c and d. As the anode, the electrode is first discharged from open-circuit voltage (A point) to 1 V (B point) and it is obviously seen that the peaks of the (0 0 −3) and (0 0 −6) crystal planes both weaken and shift to higher 2θ degrees of 13.4° and 26.8°, respectively. Upon further insertion of Na ions to 0.5 V (C point), the characteristic peaks of KCM vanish; meanwhile a broad XRD peak around 16° and some traces of the hydrated phase are detected. It is deduced that this broad peak should also be caused by ion exchange between K and Na which results in P3 substitution. At a discharge cut-off voltage of 0 V (D point), the electrode shows almost the same XRD patterns as the black line reference which indicates that a further amorphization reaction occurs. Then the voltages are increased to 0.8 V (E point) and 1.4 V (F point), and the peaks of KCM and P3 substitution no longer appear except for some traces of manganese oxides. At the end of the first charge at 2 V (G point), it is difficult to find the difference between the electrode and the black reference line besides a small quantity of hydrated phases. The XRD patterns of the second charge/discharge process show the same trend as the first cycle as shown in Fig. S10 (ESI†). Therefore, when KCM plays a role as an anode of NIBs, the pristine KCM gradually vanishes and an amorphous substance takes a leading part in the subsequent electrochemical process.

Encouraged by the bifunctional Na-storage abilities as presented above, a novel KCM-based Na-ion full battery was assembled afterwards. Pre-charged and pre-discharged KCM electrodes (4.6 and 0 V *vs.* Na$^+$/Na) are employed as the cathode and anode for the purpose of reducing the polarization and irreversibility effect in the first charge/discharge process.[12] The discharge capacity gradually increased from 58.6 to 71.6 mA h g^{-1} and average voltages over 2.5 V are simultaneously exhibited (Fig. 5a) at a constant current of 100 mA g^{-1} in a wide voltage range between 0.6 and 4.2 V. The KCM mass loadings on the cathode and anode before pretreatment are separately 1.10 mg and 1.15 mg. The energy density of the full battery is calculated to be 91 W h kg^{-1} based on the total mass of KCM on both the cathode and anode. As shown in Fig. 5b and Fig. S11a (ESI†),
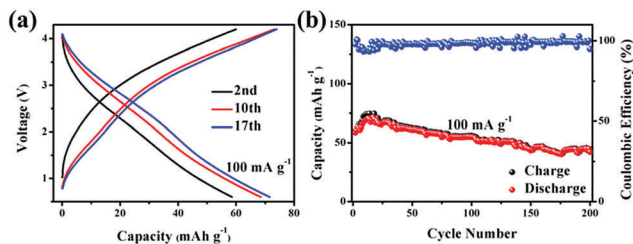
Fig. 5 (a) Charge–discharge curves of a 2025 coin-type KCM-based full cell at 100 mA g^{-1}. (b) The cycle performance of the full cell at 100 mA g^{-1}.

the battery can still deliver satisfactory electrochemical performances including a retained discharge capacity of 54.9 mA h g^{-1} after 100 cycles and a considerable average voltage of 2.8 V. Even after 200 cycles, a discharge capacity of 42.2 mA h g^{-1} can still be delivered. It is worth stressing that the coulombic efficiencies after the gradual activation process are all close to 99% which suggests a high reversibility of the KCM-based full battery. The rate ability of the KCM-based battery from 100 to 1000 mA g^{-1} is displayed in Fig. S11b and c (ESI†) and a discharge capacity of 31.9 mA h g^{-1} is still exhibited at 1000 mA g^{-1}. Table S4 (ESI†) lists the comparison between the KCM-based full battery and some existing Na-ion batteries, and it could be found that the results presented here have the advantages of a high working voltage and considerable theoretical energy density. In addition, another KCM/sodiated-Sb$_2$O$_3$ full battery is also built which provides a solution method for the purpose of direct use of K-containing compounds as cathodes for Na ion full batteries through the metal–alloy reaction between the K ion and Sb–Na alloy.[24] The battery also undergoes an activation process and delivers a maximum discharge capacity of 99 mA h g^{-1} at 100 mA g^{-1} together with a retained capacity of 70 mA h g^{-1} after 100 cycles (based on the cathode mass). The related description and figures are displayed in the ESI† (Fig. S12).

Conclusions

In summary, layered P3-type KCM is synthesized by a facile and mild sol–gel method for the first time. As is expected, KCM can play roles both as a cathode and an anode at two different potential windows (1.6–4.6 V, 0–2 V) for NIBs with satisfactory electrochemical performances. When employed as the cathode of NIBs, KCM can exhibit a considerable discharge capacity of 114 mA h g^{-1} and suitable average voltages over 3 V at a constant current density of 100 mA g^{-1}. As the anode, KCM not only delivers a safe average potential of 0.53 V and a considerably high discharge capacity of 174 mA h g^{-1}, but also shows a superior cycle-life of 950 cycles with a retained capacity of 73 mA h g^{-1} at 500 mA g^{-1}. Moreover, an innovative KCM-based Na ion full battery with satisfactory electrochemical properties, including a remarkable energy density of 91 W h kg^{-1} and a long cycle life of 100 cycles, is also successfully assembled. The experimental results suggest that the P3-type layered KCM sufficiently satisfies the bifunctional requirements of electrode materials which would significantly decrease the cost by avoiding multiple production

equipment and extra raw materials. Additionally, the work presented here will provide a new idea for the synthesis of related high-performance bifunctional electrode materials for NIBs.

Conflicts of interest

There are no conflicts to declare.

Acknowledgements

Notes and references

1 F. Cheng, J. Liang, Z. Tao and J. Chen, *Adv. Mater.*, 2011, **23**, 1695–1715.
2 Q. Zhang, E. Uchaker, S. L. Candelaria and G. Cao, *Chem. Soc. Rev.*, 2013, **42**, 3127–3171.
3 X. Xiang, K. Zhang and J. Chen, *Adv. Mater.*, 2015, **27**, 5343–5364.
4 H. Wang, P. Hu, J. Yang, G. Gong, L. Guo and X. Chen, *Adv. Mater.*, 2015, **27**, 2348–2354.
5 Y. Li, Y. Lu, C. Zhao, Y.-S. Hu, M.-M. Titirici, H. Li, X. Huang and L. Chen, *Energy Storage Mater.*, 2017, **7**, 130–151.
6 Y. Li, Z. Yang, S. Xu, L. Mu, L. Gu, Y.-S. Hu, H. Li and L. Chen, *Adv. Sci.*, 2015, **2**, 1500031.
7 D. Su, S. Dou and G. Wang, *Chem. Mater.*, 2015, **27**, 6022–6029.
8 W. Zhang, Y. Liu, C. Chen, Z. Li, Y. Huang and X. Hu, *Small*, 2015, **11**, 3822–3829.
9 K. Kaliyappan, J. Liu, A. Lushington, R. Li and X. Sun, *ChemSusChem*, 2015, **8**, 2537–2543.
10 Y. Liu, N. Zhang, L. Jiao, Z. Tao and J. Chen, *Adv. Funct. Mater.*, 2015, **25**, 214–220.
11 Y. Wang, R. Xiao, Y.-S. Hu, M. Avdeev and L. Chen, *Nat. Commun.*, 2015, **6**, 6954.
12 S. Guo, H. Yu, P. Liu, Y. Ren, T. Zhang, M. Chen, M. Ishida and H. Zhou, *Energy Environ. Sci.*, 2015, **8**, 1237–1244.
13 P.-F. Wang, Y. You, Y.-X. Yin, Y.-S. Wang, L.-J. Wan, L. Gu and Y.-G. Guo, *Angew. Chem., Int. Ed.*, 2016, **55**, 1–6.
14 L. Mu, S. Xu, Y. Li, Y.-S. Hu, H. Li, L. Chen and X. Huang, *Adv. Mater.*, 2015, **27**, 6928–6933.
15 Y. Liu, Y. Qiao, W. Zhang, H. Xu, Z. Li, Y. Shen, L. Yuan, X. Hu, X. Dai and Y. Huang, *Nano Energy*, 2014, **5**, 97–104.
16 R. Chen, P. Zavalij and M. S. Whittingham, *Chem. Mater.*, 1996, **8**, 1275–1280.
17 C. Delmas, C. Fouassier and P. Hagenmuller, *Physica B+C*, 1980, **99**, 81–85.
18 M. Butel, L. Gautier and C. Delmas, *Solid State Ionics*, 1999, **122**, 271–284.
19 L. Xu, Q. Jiang, Z. Xiao, X. Li, J. Huo, S. Wang and L. Dai, *Angew. Chem.*, 2016, **128**, 5363–5367.

20 V. Subramanian, H. Zhu, R. Vajtai, P. M. Ajayan and B. Wei, *J. Phys. Chem. B*, 2005, **109**, 20207–20214.

21 Q. Tong and J. Lian, *J. Electrochem. Soc.*, 1997, **144**, 4110–4118.

22 T. Zecheru, A. Lungu, P.-Z. Iordache and T. Rotariu, *Combust., Explos. Shock Waves*, 2013, **49**, 204–214.

23 M. M. Rahman, A. M. Glushenkov, T. Ramireddy and Y. Chen, *Chem. Commun.*, 2014, **50**, 5057–5060.

24 P. E. Mason, F. Uhlig, V. Vaněk, T. Buttersack, S. Bauerecker and P. Jungwirth, *Nat. Chem.*, 2015, **7**, 250–254.

25 R. Houghton, *Emergency Characterization of Unknown Materials*, CRC Press, Boca Raton, FL, USA, 2007, p. 89.

26 E. R. Burkhardt, *Potassium and Potassium Alloys. Ullmann's Encyclopedia of Industrial Chemistry*, Wiley-VCH, Weinheim, 2006, pp. 4–6.

27 X. Chen, X. Zhou, M. Hu, J. Liang, D. Wu, J. Wei and Z. Zhou, *J. Mater. Chem. A*, 2015, **3**, 20708–20714.

28 M. D. Slater, D. Kim, E. Lee and C. S. Johnson, *Adv. Funct. Mater.*, 2013, **23**, 947–958.